Three Dimensional Printing of Tungsten Carbide-Cobalt using a Cobalt Oxide Precursor [†]

Brian D. Kernan, Emanuel M. Sachs
Department of Mechanical Engineering
Mark A Oliveira, Michael J. Cima
Department of Materials Science & Engineering
Massachusetts Institute of Technology
Cambridge, MA 02139

Abstract

Tungsten Carbide 10 wt% Cobalt parts were formed by Slurry-based Three Dimensional Printing (3DP[TM]). The slurry contained a mixture of Tungsten Carbide and Cobalt Oxide powders, as well as dispersing and redispersing agents. The cobalt oxide is fully reduced to cobalt metal during the early stages of the sintering process. A new binder system, polyethylenimine, is described for use with powders with acidic surfaces, such as WC. Sintered densities approach the theoretical values for WC-10% Co, and the microstructures produced are similar to those of conventionally processed (press and sinter) materials. Up to four parts were produced in a single print run using a layer thickness of 25 µm, with good dimensional agreement between them, and within the range of target dimensions after sintering.

I. Introduction

Tungsten Carbide - Cobalt is widely used due to its high strength, hardness and stiffness at high temperature, particularly in metal working and mining industries and wear coating applications. Fabricating WC-Co parts is usually done by die compaction with high associated tooling costs.[1] Following compaction, liquid phase sintering is used to achieve high density.[2] The ability to quickly fabricate small batches of prototype parts for design iterations, testing or small-scale production runs has been an impetus for the development of various layer-based manufacturing or Solid Freeform Fabrication (SFF) techniques. [3-9]

SFF of WC-9wt% Co has been previously explored by selective laser sintering of both mixed and mechanically alloyed <25 to 50 µm WC and 2-4 µm Co powders to form thick 2-D layers, but not 3 dimensional parts.[10] In metal cutting applications, small (1 micron) WC grains are needed for adequate toughness; while in wear applications, larger WC grains are tolerable. Our primary aim was applications involving metal cutting inserts (milling, turning, etc.), so micron or sub-micron powders delivered via a slurry were necessary.

Slurry-based Three Dimensional Printing [11-13] (3DP[TM]) is another SFF technique. In 3DP[TM], a ceramic powderbed is formed by jetting a slurry through a small diameter nozzle

---

which is raster-scanned over a porous substrate, forming a thin slip cast layer of material. After drying, a binder material is ink-jet printed into the powder bed to form the layer geometry; followed by a second drying step. This process is repeated, building each layer on top of the previous one, until the part is completed. Sufficient binder must be printed to not only form the layer geometry, but to also penetrate through the thickness of the top slip cast layer to the layer below and knit the layers together. The regions of unprinted material serve as support for the printed regions, enabling formation of complex geometries, such as internal cavities, passages or negative draft angles. After printing is complete, the binder is cured and the parts are then retrieved from the powderbed in a process called redispersion. During redispersion, water is slowly wicked into the powder bed until the pore space is saturated. Those areas where binder is printed remain held together, while those areas without binder swell and break up by osmotic pressure and can be washed away, revealing the printed part. A low power ultrasonic bath aides in removing powder from deep crevasses.

There are several aspects that make a slurry useable in 3DP^{TM}. It must produce a body with a green density of 45% or greater for good sinterability. The slurry should slip cast slow enough so that the inter-arrival time of slurry lines during deposition is about 1/10th the time to slip cast a single line. This allows for a process called line merging, where the flatness of the bed is improved greatly when the slurry from several successive lines merge in a "wet region" before slip casting completely, as described by Polito.[14] (Bed flatness is quite important for good surface finish; a rough powderbed can cause migration of the binder along the powderbed surface in the direction of the slurry lines by capillary induced effects.) Further, the slurry must be able to be jetted through a small diameter nozzle for many hours without clogging or changing flow rate. Lastly, the unprinted regions of the powder bed must easily redisperse in water or other liquid after binder curing to enable part retrieval.

Although we did pursue both cobalt metal[15] and cobalt oxide material systems, this article will show results from the cobalt oxide route. The challenges faced in 3DP^{TM} of Tungsten Carbide-Cobalt Oxide include reducing the cobalt oxide to cobalt metal in typically sized WC-Co cutting inserts, making a suitable slurry of mixed WC and cobalt oxide powders, and development of a suitable binder material. Each of these subjects will be explained in one of the following sections; section II on oxide reduction, section IIIA on slurry, section IIIB on binder. Section IIIC will deal with 3DP^{TM} processing and show several green parts, and finally section IV will show some sintered properties and microstructures.

II. Cobalt Oxide Reduction - Thermodynamics and Kinetics

The primary reasons for pursuing the use of cobalt oxide was to avoid concerns about the chemical reactivity or corrosion of cobalt metal at various stages of the process (i.e. slurry milling, printing aqueous binder, and redispersing in water),[16] and to avoid the magnetic properties of cobalt metal powder in the slurry media. Since the oxide is already formed, there is no concern about reactions occurring during processing that would change the nature of the slurry. Cobalt oxide exists in two forms, CoO, which has the NaCl structure, and Co_3O_4, a normal spinel. The spinel powder was used in this work because it was available in

an appropriate size and purity. Quite recently, CoO has been used to form nano-grained WC-Co particles, which were converted to dense coatings via thermal spray.[17]

Because cobalt oxide was used rather than cobalt metal, there is a modest penalty in the green density after the cobalt oxide has been reduced to cobalt metal. The densities of cobalt and Co_3O_4 are 8.90 gm/cc and 6.11 gm/cc respectively. Thus, one cc of Co_3O_4, which is 73% Co by weight, will be 6.11*0.73/8.9 = 0.5 cc of Co after complete reduction. For the final mixture of WC-10 wt% Co, a mixture of WC-13.2 wt% Co_3O_4 or 28 vol% Co_3O_4 was used. For this mixture, the powder volume after oxide reduction will be (1-0.28 * 0.5) = 0.86 that of the green volume. Thus, a slip cast density of 52% or greater is desired to achieve good sintered density.

Reduction of the cobalt oxide phase to cobalt metal is a critical step in the post-processing of printed parts. Thermodynamically, reduction is quite easy to achieve, as can be seen by comparison of the Gibbs free energy of cobalt oxide and water at 400 ^{o}C, table 1. The data for Fe_3O_4 is also shown for reference. The oxidation reaction of cobalt to cobalt oxide has the least negative free energy, so it is the least favorable reaction, or conversely, the reduction of the oxide to metal is most favored.

Table1. Thermodynamic data for Co_3O_4, H_2O and Fe_3O_4.

Reaction	ΔH_o^{298} (kJ/mol O_2)	ΔS_o (J/mol O_2)	ΔG at 400°C
3/2 Co + O_2 $\Rightarrow$ 1/2 Co_3O_4	-452.8	-192.95	-323
2 H_2 + O_2 $\Rightarrow$ 2 H_2O	-484	-89.4	-423
3/2 Fe + O_2 $\Rightarrow$ 1/2 Fe_3O_4	-558.8	-170.5	-444

The main concern is therefore the kinetics of reducing small particles of the oxide to metal, particularly in modestly thick bodies, at time scales amenable to sintering cycles. Figure 1 shows a TGA curve of as received Co_3O_4 powder reduced in Ar -5%H_2. The sample (~70 mg) was heated from room temperature to 600 ^{o}C at 3 ^{o}C/min. Oxide reduction begins at around 280 ^{o}C and is essentially completed by 420 ^{o}C. The weight remaining after reduction is 73.7%, indicating near complete reduction of the oxide to metal. Oxide reduction in the presence of WC was confirmed by mixing 86.8 wt% WC and 13.2 wt% cobalt oxide. The powders were milled in DIW for ~20 hrs and slip cast onto a porous plaster block. After slip casting, the sample was put in a desiccator overnight. A piece of the slip casting was then subject to the same TGA cycle as the Co_3O_4 powder, shown in Figure 2. The weight remaining is 96.5%, whereas theoretically 96.8% should remain. The extra mass loss can be attributed to water loss during the early part of the burnout (0.02 wt%) and perhaps partial reduction of cobalt hydroxide that might be formed on surfaces during the milling process in water. In the presence of WC, the temperature range for oxide reduction begins at about the same temperature (280 ^{o}C) as the case without WC present, but slight weight loss continues above 420 ^{o}C. The increase in temperature for complete reduction may be because of the higher packing fraction in the slip cast piece of WC-cobalt oxide vs. the loose packing of dry cobalt oxide powder, in which case gas flow is easier in the larger pores of the loose packed powder.
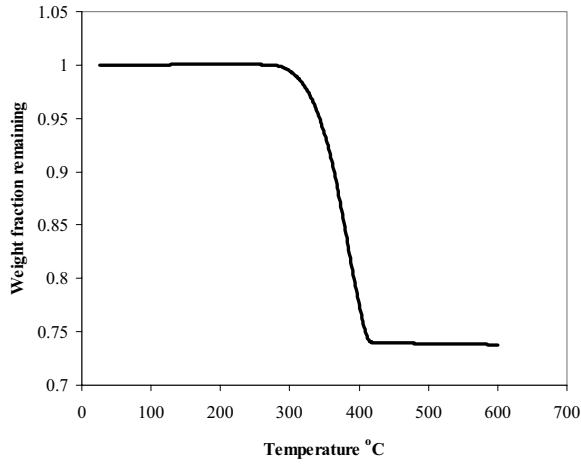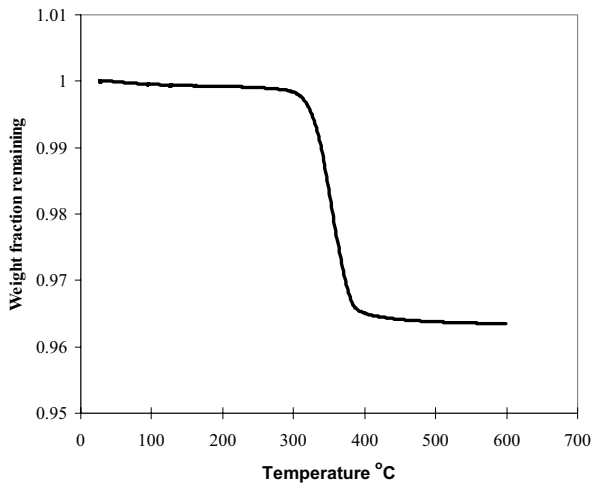
Figure 1. TGA of Co_3O_4 in Ar-5%H_2.

Figure 2. TGA of WC-13.2w% Co_3O_4 in Ar-5%H_2.

The kinetics of the reduction process can be viewed in the following analysis. We assume that the diffusion of gas in the powderbed is the rate-limiting step in calculating the time required for reducing the printed part. For reduction of a half-thickness, t, we first calculate the diffusivity of an H_2 - H_2O mixture according to;

$$D_{H2,H2O} = \frac{\left(1x10^{-3}\right)T^{1.75}}{P\left(V_{H2}^{1/3} + V_{H2O}^{1/3}\right)^2} \sqrt{\frac{1}{M_{H2}} + \frac{1}{M_{H2O}}} \qquad \text{eq 1}$$
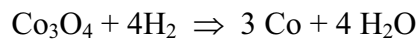
where V is the atomic volume and M is the molecular weight of a gas molecule (g/mol), T is temperature (K) and P is total pressure (atm).[19] Using T = 673K, P = 1 atm, V_{H2} = 7.07, V_{H2O} = 12.7, M_{H2}=2 g/mol and M_{H2O}=18 g/mol, then $D_{H2,H2O}$ = 3.69 cm²/sec.

Next, calculate the flux of gas across a half-thickness of powder bed with a linear concentration gradient of 1 atm at 673K assuming ideal gas behavior. For this model, assume that the powder bed is unreactive, and on one side there is a pure hydrogen atmosphere and on the other side a pure water vapor atmosphere each maintained at 1 atm. Across the bed at steady state, there will be a flux of gas

$$J = -D_{eff}\frac{dc}{dx}\frac{1}{\tau} = -D_{eff}\frac{\Delta c}{\Delta x}\frac{1}{\tau}$$
eq 2

where Δc = 1.81e-5 mol/cm^3 , Δx = t = 0.3 cm, and τ is the tortuosity, which is assumed to be 3. Then J = -7.42e-5 mol/cm^2·sec.

Next, calculate the mass of cobalt oxide and hydrogen gas that are reacted in the half-thickness of powderbed. The mass of cobalt oxide in a 1 x 1 x 0.3 cm volume of WC-13.2 wt% cobalt oxide powderbed at 53% density is 0.271g, which is 1.14e-3 moles. The reduction reaction is

$$Co_3O_4 + 4H_2 \Rightarrow 3\ Co + 4\ H_2O$$

so by mass balance 4.56e-3 moles of H_2 are needed to reduce the oxide. Assuming the limiting case that all the hydrogen gas diffuses through the half thickness of powderbed,

$$-J = n / A \bullet t$$
eq 3

where n is the number of moles of diffusing gas (4.56e-3), A is the cross sectional area (1 cm^2) and t is the time for diffusion (sec). Rearranging eq 3 and solving for t, we find that t = 61.5 seconds. Assuming a hydrogen gas pressure of 48 torr (5% of 1 atm), rather than 1 atm, the time is approximately 20.5 minutes, which is within the time range allowable in an industrial setting.

While this model is not exact, as it does not account for the reduced tortuosity of the reacted powderbed, or the reactivity of the powderbed; it does provide us with an upper limit of the reaction time, assuming that gas diffusion in the powderbed is the rate limiting step.

III 3DP Processing: A. Slurry Development

Two different slurries were used; a water-based slurry achieved some initial success, however better results were found with an isopropyl alcohol (IPA) based slurry, which will be shown here. The slurry formulation is shown in Table 2. Two levels of solids loading are shown for the IPA slurry, 25% and 18% of solids by volume. The WC used was Valenite 1399 powder with an average size of 0.8 μm. The cobalt oxide powder used was Umicore 73 (73.5% Co with 0.036 wt% Ni and 0.014 wt% Fe impurities, 95% Co_3O_4/5%CoO) with an average size of ~1-2 μm. Polyethylene glycol (mw 200) was used as the redispersion aid to increase the osmotic pressure in the unprinted regions of the powderbed.[20] The slurries were

balled milled in a polypropylene container using magnesia stabilized zirconia milling media. Milling times were typically 18-22 hrs. After milling, the slurry was passed through a 30 μm nylon screen to remove any gross agglomerates.

Table 2. Slurry Formulations.

	Alcohol system	Alcohol system
Powder loading, vol%	25%	18%
Weight %:		
WC	72.80	67.34
Co_3O_4	11.08	10.25
Dispersant	0.42 Polyvinylpyrolidone	0.39 Polyvinylpyrolidone
PEG 200	0.67	0.62
Liquid	IPA	IPA
Slurry density (g/cc)	3.85	3.00

The viscosity of the 25 vol% IPA slurry was measured on a parallel plate viscometer over shear rates ranging from 1 to 3000 sec^{-1} at 22 ^oC, shown in Figure 3. Initially, the slurry is slightly shear thinning but the viscosity becomes constant at 5 cP above a shear rate of 20 sec^{-1}. However, the viscosity at low shear rates is still quite low and the slurry is fairly well behaved.
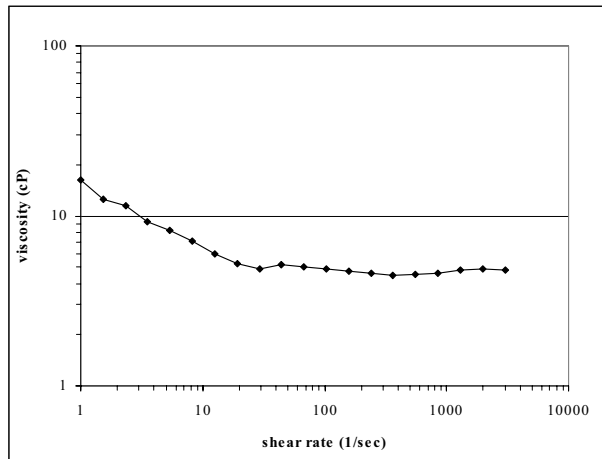

Figure 3. Viscosity of 25 vol% WC-Co3O4 slurry in IPA

The slurry was jetted through a 127 μm diameter alumina nozzle (Gaiser Tool Co., Ventura, CA) onto porous alumina substrates to form powderbeds. In our slurry jetting station, a linear nozzle speed of up to 2.0 m/sec can be obtained with a frequency of 5.8 lines per second deposited over a powder bed 100 mm wide. The fast turn-around time aides in obtaining a "wet region" and smooth powderbed.

To observe the layer roughness of the powder bed surface and find the density of the powder bed, jetted beds were formed using the 18 vol% IPA slurry at carriage velocities of 2

m/sec and slurry line spacings of 300 μm. A mass flow rate of 7.93 g/min yielded a layer thickness of 25 μm. Density measurements were by Archimedes' method in water after infiltrating the powderbed sample with a paraffin wax.   Layer roughness was measured by examining successive layer height profiles taken (after slurry drying) with a laser profilometer over a 3 mm wide section of the bed with readings taken every 10 μm.

The density of the IPA slurry powder bed was 53%, resulting in theoretical post-oxide reduction density of 45.6%, which met our minimum density requirement. Typical height profiles of the powder bed are shown in Figure 4. Ten consecutive layers are shown. The average surface roughness (standard deviation of layer height) of the 10 layers is 3.7 μm, and the average layer thickness was 24.3 μm. Although the surface is not completely flat, there is little periodicity to the surface that reveals the 300 μm line spacing. The wet region visible during layer formation was about 3-5 slurry lines, only one-third to half the number (10) that Polito *et al.* describe as necessary for good smoothness. [14] (In fact, the reason for using the 18 vol% slurry over the 25 vol% slurry when making powder beds was to increase the wet region). A low-angle-light optical micrograph of a typical area of the bed, Figure 5, shows that there are still some remnants of the slurry lines in the top surface, running vertically in the photo, although these are not discernable in the profilometry data.
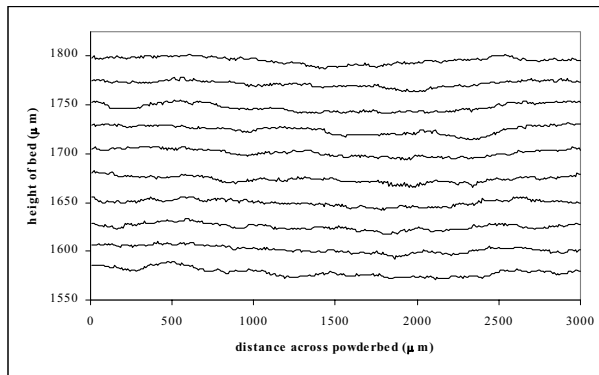

Figure 4. Laser height profiles of 10 consecutive layers formed from the 18 vol% IPA slurry.   Each line is the profile of a 3 mm section of one layer scanned perpendicular to the slurry rastering direction.

Figure 5. Top surface of jetted bed, typical region. 18 vol % slurry.

In their studies of line merging in alumina slurries, Polito *et al.* were able to form a wet zone up to 6 mm wide encompassing 30 lines with a line spacing of 200 μm. While the

3-5 line wet zone of the IPA slurry is not nearly as large, they used a layer thickness of 50 μm, versus our 25 μm. Since the time to slip cast a line is dependant on the square of the layer thickness, our results would give a wet zone of 12-20 lines at 50 μm layer thickness.

III B Binder Development

Previously in 3DP[TM], an aqueous solution of polyacrylic acid (PAA) and glycerol has been used as the binder, the glycerol serving as a cross linking agent during curing.[21] Holman *et al*,[22] showed that the basic surface of many ceramic powders adsorbs PAA. In the WC-Co_3O_4 system, the WC surface is acidic, while the Co_3O_4 surface is basic, isoelectric point pH=10.4.[23] Given that there is several times more surface area of WC powder as there is Co_3O_4 powder in the powder bed, it is more reasonable to have a binder that is strongly attracted to the WC, than one that is strongly attracted to the cobalt oxide.

Polyethylenimine (PEI, $H[NHCH_2CH_2]_n NH_2$), mw = 10K (Polysciences) was chosen as a new binder because of it's high pH in aqueous systems. Laarz and Bergstrom[24] previously found that PEI is a good dispersant for WC-Co in water based systems, and theorized that the dispersion was due to a combination of steric and electrostatic forces, so we theorized that it might make it a suitable binder. Following the method of Holman, a series of five 20 vol% WC slurries were made containing differing amounts of PEI, (5, 2.25, 0.75, 0.3 and 0 vol% PEI). The slurries were mixed for 19 hrs then centrifuged at 1150 gees for 30 minutes and the supernatant decanted and centrifuged again at 12000 gees for 60 minutes, and decanted again. The residual PEI concentration in the supernatant was measured by nitrogen analysis, and the remaining PEI was assumed to be adsorbed onto the WC surface. The adsorption profile of PEI onto WC powder is shown in Figure 6, along with the data pertaining to alumina from Hollman, *et al*. The y-intercept value shows the amount of binder (mg/m^2) adsorbed onto the powder surface at the point were there is no binder left in solution. The plot shows the continued increase in adsorption vs. the residual solution concentration. There is a strong tendency for the PEI to bind to the WC surface, nearly as strong as for PAA to bond to alumina, however, in the WC case, PEI continues to adsorb onto the WC as the solution concentration is increased.
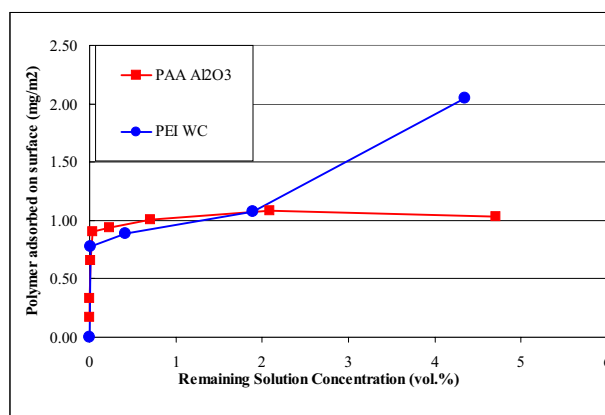

Figure 6. Binder adsorption onto ceramic surfaces. PEI adsorbs strongly to WC and PAA adsorbs strongly to Al_2O_3. PAA data from Holman et al.[22]

The binder solution used in printing is 2.5 wt% PEI (2.4 vol%) in deionized water with 0.25 wt% glycerol added as a cross linking agent. The binder solution has a pH = 9.5, and it's viscosity is 1.1 cP, making it easily printable in our drop-on-demand printhead.[25] The binder is cured in a flowing argon atmosphere at 1 atm. in an oven held at 150 °C for 1 hour. While we have no direct chemical evidence of cross linking, freshly retrieved (still wet) 0.3 μl cured binder droplets in WC-Co$_3$O$_4$ powder beds were flexible without the presence of glycerol, but stiff with the presence of glycerol. Further, cured binder droplets with glycerol were much stronger than uncured binder droplets with glycerol.

III C Processing Parameters

Typical slurry deposition parameters for the printed parts were similar to those given in section IIIA. Between layer jetting cycles, the flow of slurry was interrupted to conserve slurry. Twenty foundation layers were deposited before printing the first part layer, and five top layers were made after the last printed part layer. The slurry and binder were both dried for 25 seconds at 60 °C in a convection oven after deposition. The binder was applied in two steps, the first is the traced (or vector) outline of the layer, the second is a raster fill of the interior. Up to four separate nozzles, each producing one part, were used for several builds. The initial binder dosage after drying was 3.9% of the pore space in the slip cast bed, achieved during raster printing by using a 55 μm drop spacing at a frequency of 1272 Hz, a printhead traverse speed of 7 cm/sec, a 40 μm raster line spacing and a flow rate of 3.2 mg/min. A similar dosage was applied in the vector pass. The vector printed lines were offset 50 μm to the inside of the actual part geometry to account for the thickness of printed line.

III D Green Parts

Several geometries of green parts were printed. One was a simple square shaped insert, 16.21 mm on a side and 6.20 mm thick (252 layers), was made using the 18 vol% slurry. Previous sintering experiments on smaller printed parts had shown that the scaling factor for shrinkage in the thickness was 1.3 and in the width and length was 1.27. Thus the simple square insert would be 12.7 mm (1/2") square and 4.77 mm (3/16") thick when sintered, typical of the size of many common indexable cutting inserts. (The total volumetric reduction assuming 100% final density and the 1.27 x 1.27 x 1.3 shrinkage factors yields a starting density of 47.6%, slightly greater than the 45.6% measured by Archimedes' method on the jetted bed.) A tapered groove 0.65 mm deep extends along the perimeter of both the top and bottom of the part, simulating a chip breaking groove in a double sided cutting insert. The goal of printing this part was primarily to confirm that the cobalt oxide could be completely reduced, good microstructures developed in objects the size of cutting inserts, and to make some geometrical measurements in the green and fired state.

One of the green square inserts is shown in Figure 7. Close up views of the top and bottom surfaces of the part are shown in Figure 8 (a&b). The top surface, Figure 8a, is discernable by the relatively smooth surface, with evidence of slurry line rastering in the vertical direction. The bottom surface, Figure 8b, is discernable by the bleed through of the array of binder droplets, each binder droplet forming a spheroid on the bottom surface. Table 3 shows the average dimensions of the green parts, they are just slightly larger than the target

size. (Measurements were taken using a stereo-microscope with a stage micrometer accurate to 0.01 mm). The locations of the dimensions are shown in Figure 9. The difference between the actual and target dimensions are mostly less than one binder droplet diameter, so good dimensional control has been demonstrated in this simple part. There are some delaminations, or partial chipping, in the parts in the area of the cutting edge, indicating that a higher binder dosage was needed.
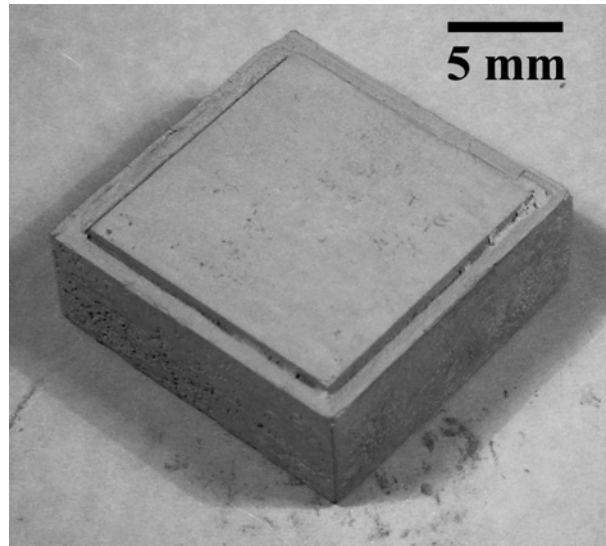

Figure 7. Square 16.2 mm x 6.2 thick insert. Shown after part retrieval.
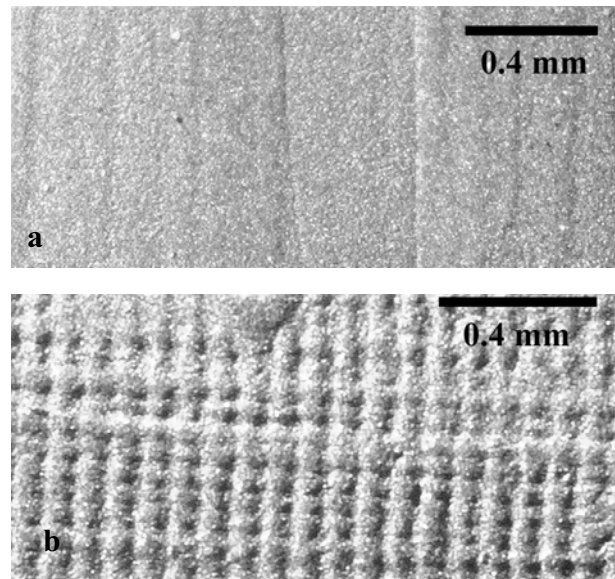

Figure 8. a) Top surface of square insert. Slurry rastering direction is vertical. No binder deposition is visible. b) Bottom surface of square insert. Slurry rastering direction is horizontal. Binder bleed through is evident by array of droplets.

Table 3. Measured dimensions of green square inserts.

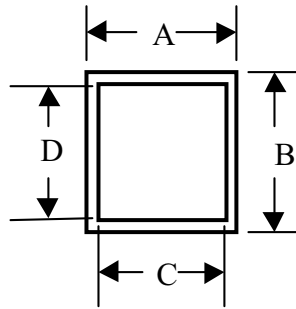| Dimension	A (mm)	B (mm)	C (mm)	D (mm)
Average	16.24	16.23	13.68	13.67
Range	0.09	0.17	0.07	0.06
Target	16.21	16.21	13.61	13.61
Deviation	0.03	0.02	0.07	0.06

Figure 9. Location of dimensions shown in Table 3 for square insert.

A second set of four parts was the top 80 layers (2mm thick green part) of a CNMG style cutting insert. The perimeter of the part is a diamond with rounded corners and a through hole for mounting and there is much more surface detail present in the top layers than in the simple square insert. The diamond sides are 16.27 mm apart with an acute angle of 80°, and the center through hole has a diameter of 6.61 mm. The slurry parameters were the same as for the simple square insert, however a higher binder dosage was used, 4.4 % of the pore space, in order to get better knitting of the layers.

The four green printed parts are shown together in Figure 10. Figure 11 shows a top view of one of the inserts. Shown in Figure 12 are: the area around the sharper radiused corner (12a), one of the edges showing the chip breaking groove (12b), one quadrant of the countersunk through hole (12c), and the side edge of the part (12d). Printed and target dimensions are shown in Table 4. Locations of measured dimensions are shown schematically in Figure 13. Dimensions A and B are exterior dimensions, while the other dimensions are interior dimensions. Exterior dimensions will become larger than target with insufficient offset, while interior dimensions become smaller with insufficient offset. It is clear from the measurements in Table 4 that a larger offset value should have been used for printing this geometry. Since more binder was used in printing the CNMG insert than in printing the square insert, this accounts for some of the difference in part size. Further indication of insufficient offset is that the recessed text (which should read '80', '2' and 'MP') within the 3 recessed areas is mostly unreadable. The range of actual values for the four parts is quite good, a maximum of 0.07 mm, with most dimensions 0.04 mm or less, demonstrating good reproducibility in a highly complex part.
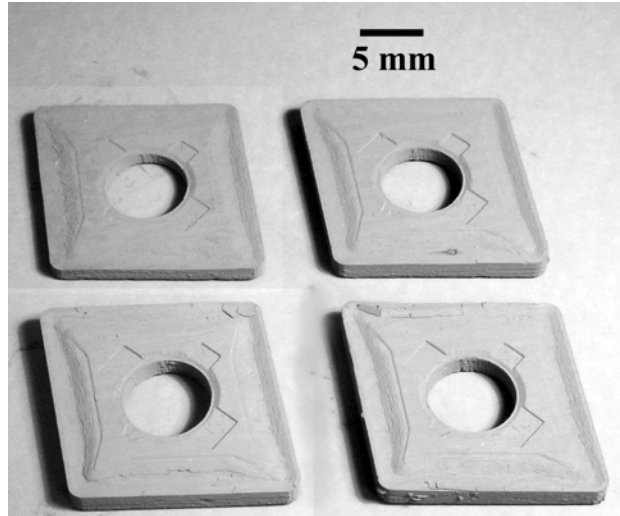
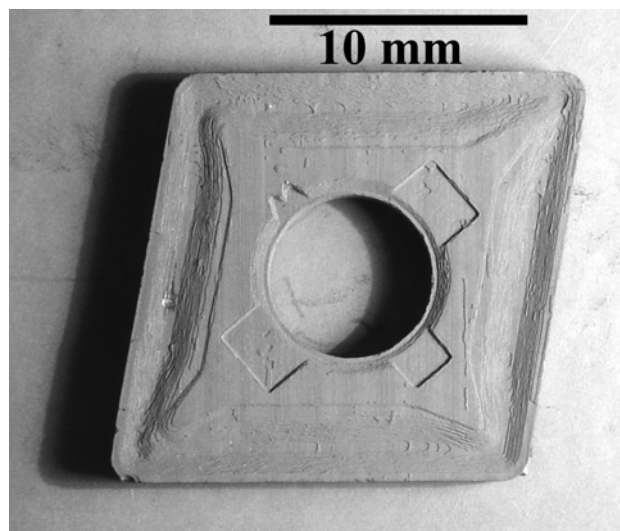Figure 10. Four printed CNMG style inserts.

Figure 11. Top view of one CNMG style insert.

Comparing the quality of the printed regions in Figure 12, it is evident that some regions are expressed better than others. The countersunk area of the through hole (figure 12c) is among the best produced geometry on the part. The consecutively larger circles are well defined, producing a uniform stair step. The area to it right of the through hole, which slopes back down toward the chip-breaking groove, is not as clean. Several layers appear to have areas that have been washed away, as evidenced by the wavy stair step, particularly the top most layer (along the line marked "A"). The critical difference between the two areas may be the size of the horizontal step. In the countersunk region, the horizontal step is 45 μm, which is less than the thickness of one printed vector line, ~70 μm. In the sloped region the horizontal step is 80 μm for most of the steps, but 356 μm for the long step where significant washing out occurred, as noted by points A and B in the figure. The central region

of Figure 12b is similar to the right side of Figure 12c. It is possible that a higher binder dosage will preserve these geometries more precisely.
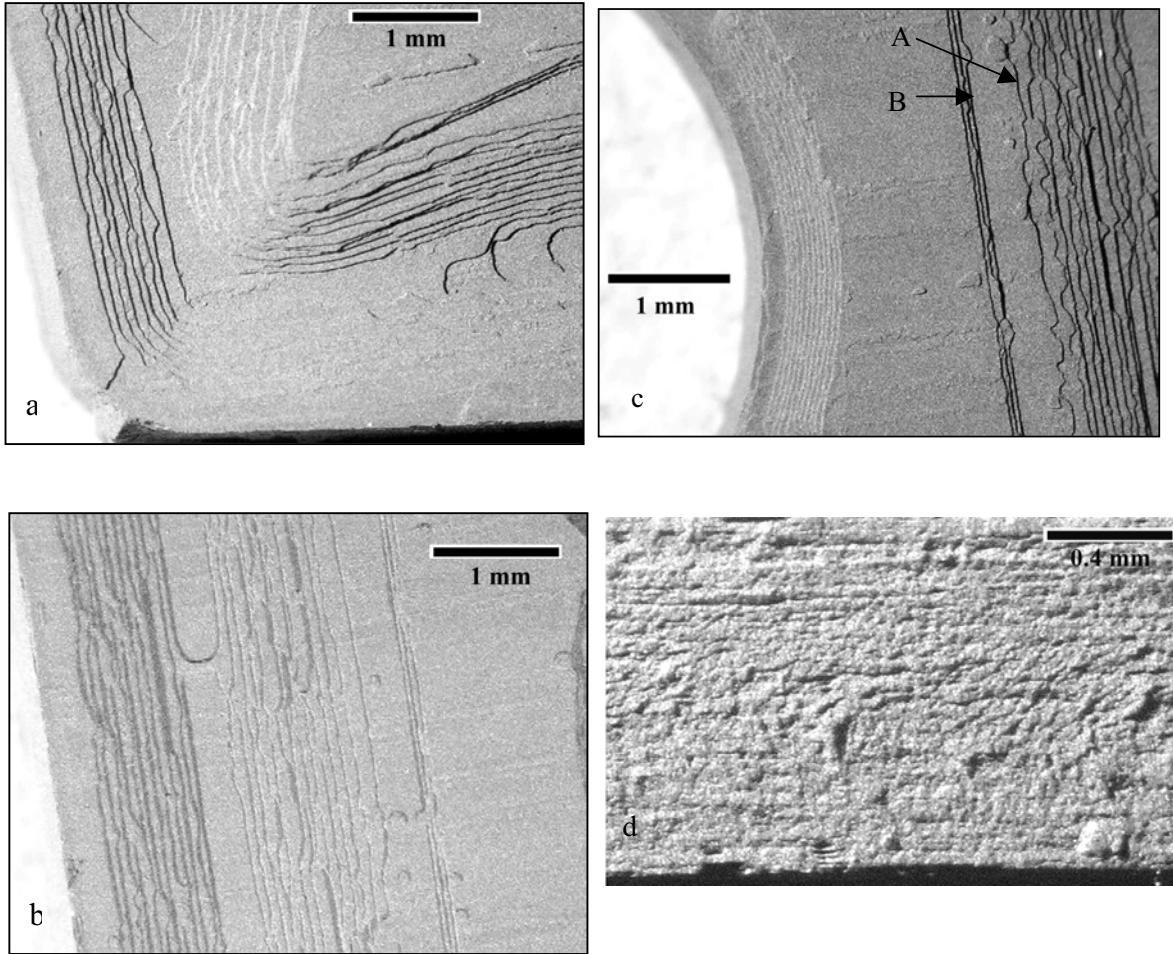

Figure 12 (a-c). Images of printed CNMG style insert. a) 110° corner. b) edge, chip breaking groove top land. c) through-hole with counter sink, top land and slope back to chip breaker. d) edge (side view), slurry rastering direction is out of the page.

Table 4. Measured dimensions of CNMG style insert (all dims in mm).

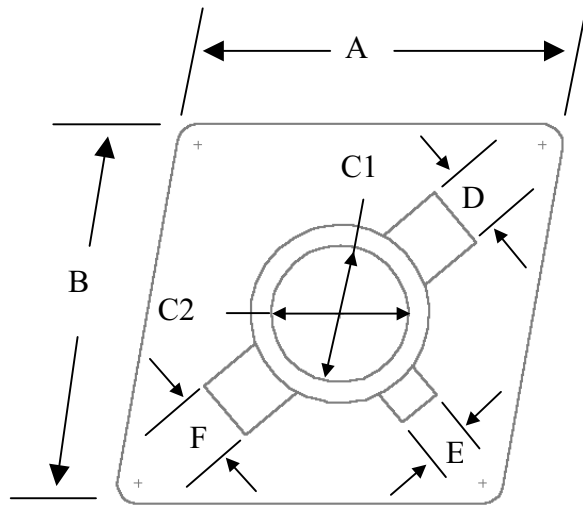| Dimension	A	B	C1	C2	D	E	F
Average	16.16	16.15	6.47	6.45	2.99	2.00	2.98
Range	0.02	0.02	0.07	0.05	0.03	0.04	0.04
Target	16.08	16.08	6.61	6.61	3.10	2.13	3.10
Deviation	0.08	0.07	-0.14	-0.16	-0.13	-0.13	-0.12

Figure 13. Schematic showing location of measured dimension given in table 4.

The side of the part, Figure 12d, is relatively flat, although there is evidence of layering in this view where all of the layers line up directly (layers run horizontally). Certainly, the side is not as flat as the top or bottom, however, the low angle lighting exaggerates the surface roughness. Shown is the side of the part that is perpendicular to the slurry forming raster direction (also parallel to the binder rastering direction). In this view, the effects of a rough powder bed surface would be maximized, because the slurry lines are running out of the page.

IV Sintered structures

The large double sided insert was reduced in a series of slow ramps, with 1 hour holds every 56 ^{o}C (100 ^{o}F) between 93 ^{o}C (200 ^{o}F) and 371 ^{o}C (700 ^{o}F) and another hold at 510 ^{o}C (950 ^{o}F) in a flowing partial pressure of 30 milliTorr of H_2., which was somewhat more aggressive than either the TGA or numerical model suggested was necessary. This reduction schedule is similar to the burnout process used with heavily lubed WC-Co press-and-sinter articles.[26] The part was then sinter-HIPed according to normal industrial practice for WC-10 Co articles, the HIP pressure being 800 PSI. Dimensionally, the sintered part is within 80 µm of the target square dimension (12.70 mm) after sintering, however the height is a bit low 4.52 mm actual vs. 4.77 mm target. The ASTM porosity rating is A04B00C00; so there are a small number of pores all smaller than 10 µm. The density of smaller similarly processed parts was 14.42 g/cc, which compares fairly well with conventionally processed WC-10 Co which has a density of 14.5 g/cc. Figure 14 shows the typical etched microstructure. The WC grain size is 1-4 µm, and some cobalt rich areas up to 15 µm are present. The number and size of pores, WC grain size and amount of cobalt pooling are within the range of acceptable WC-10 Co microstructures. There is some *eta* phase (W_2C) present in the microstructure (not visible in Fig 14), indicating that the part was partially decarburized during the oxide reduction process. Less aggressive oxide reduction would result in no *eta* phase.
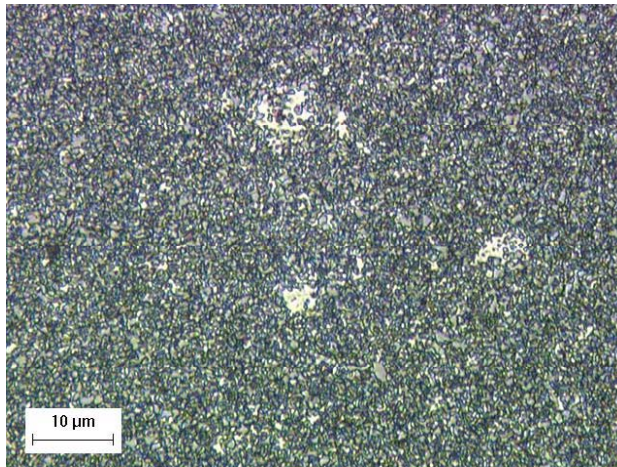
Figure 14. Etched microstructure of reduced and sintered square insert showing typical WC grain size and occasional cobalt pooling. (Micrograph courtesy of Kennametal, Inc.)

V Summary

The 3DP process has been shown to be able to produce a multitude (up to four) of both simple and complex geometry parts from a WC-cobalt oxide - IPA slurry using a polyethylenimine binder. It has been demonstrated that complete reduction of the oxide and high sintered densities and acceptable WC grain size and cobalt distribution can be achieved from the mixed WC-cobalt oxide materials in part sizes that are typical of WC-Co cutting inserts. Dimensional repeatability from part to part is excellent, and target dimensions have been met in sintered parts with simple geometries although further work is needed concerning offsetting dimensions to meet target values in complex geometries printed with higher binder dosing. Surface roughness of printed parts is good, although some wash-out of printed regions is found, indicating higher binder dosing (more than 4.4% of the pore space) may be needed. The direct manufacture of custom metal cutting tools and inserts via 3DP^{TM} is distinctly possible. Further, this route to forming fine grained WC-Co items may have implications outside of the realm of 3DP^{TM}, for instance in spray drying, slip casting or other liquid aided forming processes.

Acknowledgements

[1] K. Rodiger, H. Van Der Berg, K. Dreyer, D. Kassel, S. Orths, " Near-net-shaping in the hard metal industry," , European Conference on Advances in Hard Materials Production Proceedings (UK), 91-102 (1999).
[2] R.M. German , *Sintering Theory and Practice*, John Wiley & Sons, New York 1996.

[3] H. L. Marcus and D. L. Bourell, "Solid Freeform Fabrication Finds New Applications," *Adv. Mater. Processes*, **9**, 28-35 (1993).

[4] J. D. Cawley, A. H. Heuer, W. S. Newman, and B. B. Mathewson, "Computer-Aided Manufacturing of Laminated Engineering Materials," *Am. Ceram. Soc. Bull.*, **75** [5] 75-79 (1996).

[5] M. K. Agarwala, A. Bandyopadhyay, R. van Weeren, A. Safari, S. C. Danforth, N. Langrana, V. R. Jamalabad, and R. J. Whalen, "FDC, Rapid Fabrication of Structural Components," *Am. Ceram. Soc. Bull.*, **75** [11] 60-65 (1996).

[6] E. M. Sachs, M. J. Cima, P. Williams, D. Brancazio, and J. Cornie, "Three-Dimensional Printing: Rapid Tooling and Prototypes Directly from a CAD Model," *J. Eng. Ind.*, **114**, 481-88 (1992).

[7] D. L. Bourell, H. L. Marcus, J. W. Barlow, and J. J. Beaman, "Selective Laser Sintering of Metals and Ceramics," *Int. J. Powder Metall.*, **28**, 369-81 (1992).

[8] M. L. Griffith and J. W. Halloran, "Solid Freeform Fabrication of Ceramics via Stereolithography*," Am. Ceram. Soc. Bull.*, **79**, 2601-608 (1996).

[9] W.M. Sigmund, N.S. Bell, L. Bergstrom, "Novel powder-processing methods for advanced ceramics," J Am. Ceram Soc. 83 [7] 1557-1574 (2000).

[10] T. Laoui, L. Froyen, and J-P. Kruth, " Effect of Mechanical Alloying on Selective Laser Sintering of WC-9Co Powder," Powder Met., **42** [3] 203-205 (1999).

[11] J. E. Grau, S. A. Uhland, J. Moon, M. J. Cima, and E. M. Sachs, "Controlling Cracking of Multilayer Ceramic Bodies," *J. Am. Ceram. Soc.*, **82** [8] 2080-86 (1999).

[12] J. E. Grau, J. Moon, S. Uhland, M. J. Cima, and E. M. Sachs, "High Green Density Ceramic Components Fabricated by the Slurry-Based 3DP Process"; pp. 371-79 in Proceedings of the Solid Freeform Fabrication Symposium (Aug. 11-13, 1997). Edited by J. J. Beaman, H. L. Marcus, D. L. Bourell, J. W. Barlow, and T. Crawford. University of Texas, Austin, TX, 1997.

[13] S. A. Uhland, R.K. Holman, S. Morissette, M.J. Cima, E.M. Sachs, "Strength of Green Ceramics With Low Binder Content." *J. Amer. Ceram. Soc.* **84** [12] 2809-2818 (2001).

[14] B.F. Polito, B.N. DeBear, P.C. Saxton, E.M. Sachs, M.J. Cima "Line Merging: A Layer Deposition Technique for Fine Ceramic Powders." submitted to J. Amer. Ceram. Soc.

[15] Mark A. Oliveira "Slurry Based Three Dimensional Printing (S-3DP™) of Tungsten Carbide Cobalt," SM Thesis, Massachusetts Institute of Technology, June 2002.

[16] K.M. Andersson, L. Bergstrom " Oxidation and dissolution of tungsten carbide powder in water*," Int J. Ref. Met Hard Mat.*, **18** [2-3] 121-129 (2000).

[17] Z-G Ban, and L.L. Shaw, " Synthesis and processing of nanostructured WC-Co materials," *J. Mat Sci.*, 37 [16] 3397-3403, (2002).

[18] J.W.Evans, L.C De Jonghe, *The Production of Inorganic Materials*, New York, Maxwell Macmillan International Pub. Group, 1991.

[19] D.H. Geiger, D.R. Poirier, "Transport Phenomena in Metallurgy," Addison-Wesley Publishing Co., Reading, MA, 1973. p 467.

[20] J. Moon, J. E. Grau, M. J. Cima, and E. Sachs, "Slurry Chemical Control to Produce Easily Respersible Ceramic Powder Compacts," *J. Am. Ceram. Soc.*, **83**[10] 2401-08 (2000).

[21] J. Moon, J.E. Grau, V. Knezevic, M.J. Cima, E.M. Sachs, "Ink-Jet Printing of Binders for Ceramic Components," *J. Am. Ceram. Soc.* **85** [4] 755-762 (2002).

[22] R.K. Holman, S.A. Uhland, M.J. Cima, E. Sachs, "Surface Adsorption Effects in the Inkjet Printing of an Aqueous Polymer Solution on a Porous Oxide Ceramic Substrate. *J. of Colloid and Interface Sci,* **247**, 266-274 (2002).

[23] P.H. Tewari, A.B. Campbell, "Temperture Dependence of Point of Zero Charge of Cobalt and Nickel Oxides and Hydroxides," J. Coll Inter Sci. **55** [3] 531-539 (1976).

[24] Laarz, E., Bergstrom, L., "Dispersing WC-Co powders in aqueous media with polyethylenimine." *Int J. Ref Met & Hard Mat.* **18** (6) 281-286 (2000).

[25] Blake W. Gleason, "Positive Pressure Drop-on Demand Printhead for Three Dimensional Printing," SM Thesis, Massachusetts Institute of Technology, September, 2002.

[26] Personal communication, Dave Siddle, Kennametal, Inc., Latrobe, PA.